Dissipative Optomechanical Preparation of Macroscopic Quantum Superposition States

Dissipative Optomechanical Preparation of Macroscopic Quantum Superposition States

M. Abdi,[1,2] P. Degenfeld-Schonburg,[1] M. Sameti,[3] C. Navarrete-Benlloch,[4,5] and M. J. Hartmann[3]

[1]*Physik Department, Technische Universität München, James-Franck-Strasse 1, 85748 Garching, Germany*
[2]*Institut für Theoretische Physik, Albert-Einstein-Allee 11, Universität Ulm, 89069 Ulm, Germany*
[3]*Institute of Photonics and Quantum Sciences, Heriot-Watt University, Edinburgh EH14 4AS, United Kingdom*
[4]*Max-Planck-Institut für Quantenoptik, Hans-Kopfermann-Strasse 1, 85748 Garching, Germany*
[5]*Institute for Theoretical Physics, Universität Erlangen-Nürnberg, Staudtstrasse 7, 91058 Erlangen, Germany*
(Received 29 February 2016; published 10 June 2016)

The transition from quantum to classical physics remains an intensely debated question even though it has been investigated for more than a century. Further clarifications could be obtained by preparing macroscopic objects in spatial quantum superpositions and proposals for generating such states for nanomechanical devices either in a transient or a probabilistic fashion have been put forward. Here, we introduce a method to deterministically obtain spatial superpositions of arbitrary lifetime via dissipative state preparation. In our approach, we engineer a double-well potential for the motion of the mechanical element and drive it towards the ground state, which shows the desired spatial superposition, via optomechanical sideband cooling. We propose a specific implementation based on a superconducting circuit coupled to the mechanical motion of a lithium-decorated monolayer graphene sheet, introduce a method to verify the mechanical state by coupling it to a superconducting qubit, and discuss its prospects for testing collapse models for the quantum to classical transition.

A fundamental open question in modern quantum mechanics is how classical physics arises from it as one moves from the microscopic to the macroscopic world. Decoherence is arguably the strongest candidate for the process inducing such a transition [1]. There are, however, theories which explain this transition via so-called collapse or spontaneous reduction models and attribute it to other sources, e.g., spontaneous localization [2], quantum [3] or classical [4] gravity, or uncertainty relations on the space-time continuum [5]. Proposals for testing such models exist [6], and most of them require the preparation of massive objects either in superposition [7–9] or entangled states [10,11] (the latter also have applications for quantum information processing [12–14]). Several works have emerged proposing protocols for the preparation of such states, especially in the context of optomechanics, either probabilistically [11,15,16] or in the transient regime [17–22]. Mechanical elements, however, are exposed to high decoherence rates induced by their finite temperature environments, which demand fast, yet accurate, state preparation and certification methods [23]. With direct full-state tomography being quite challenging, some indirect reconstruction methods have been proposed [24–26].

Another way to meet the challenge of large mechanical decoherence is to generate the desired states dissipatively, that is, as robust and long-lived steady states. Here we propose a method for the dissipative preparation of a mechanical element in a superposition of two spatially separated states, together with an efficient way to verify such preparation. Our proposal, therefore, paves the way

towards experimental tests of collapse models for the quantum to classical transition.

We here consider state-of-the-art superconducting circuits and electromechanical devices to show that a highly controllable and tunable double-well potential can be engineered electrostatically, while the mechanical motion of the trapped element can be cooled to its ground state with high fidelity. Because of the shape of the potential, this ground state is a spatial-superposition state. We show how to verify its preparation via population measurements on a single qubit and discuss the avenues this opens for testing collapse models for the quantum to classical transition.

Model.—We consider the motion of a mechanical element with effective mass m moving in a symmetric double-well (DW) potential as described in terms of its position $\hat{x}$ and momentum $\hat{p}$ by the Hamiltonian

$$\hat{H}_{\text{DW}} = \frac{\hat{p}^2}{2m} - \frac{\nu}{2}\hat{x}^2 + \frac{\beta}{4}\hat{x}^4. \qquad (1)$$

Here, the double-well potential results from a combination of an inverted parabola generating a potential barrier at the origin and an attractive quartic potential that dominates at large deflections. We describe the physical origin of the parameters ν and β for our proposed implementation below and denote the eigenstates and eigenvalues of $\hat{H}_{\text{DW}}$ by $\hat{H}_{\text{DW}}|n\rangle = E_n|n\rangle$ ($n = 0, 1, 2, \ldots$).

The potential of Eq. (1) together with its eigenvalues is sketched in Fig. 1. For states with energies below the peak of the central barrier, tunneling between the wells breaks
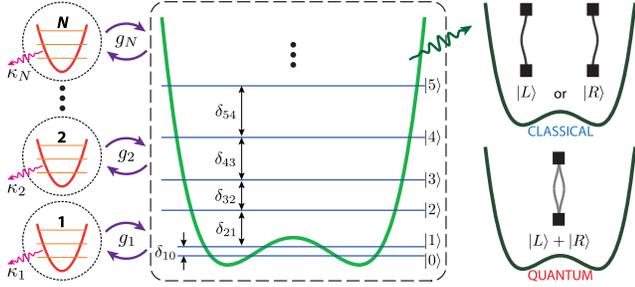
FIG. 1. Conceptual scheme of our proposal. A mechanical element moving in a shallow double-well potential with only two possible states below the central barrier is coupled to several electromagnetic modes capable of cooling its different transitions. Whereas the ground state of this potential is a spatial superposition of left and right deflections, $|0\rangle = (|L\rangle + |R\rangle)/\sqrt{2}$, without sideband cooling on several transitions only the classical mixture $(|L\rangle\langle L| + |R\rangle\langle R|)/2$ would be accessible.

the left or right degeneracy, and the eigenstates of the system are formed by symmetric and antisymmetric superpositions of states localized in the two individual wells. These localized states are well approximated by eigenstates of harmonic potentials with frequency $\omega_0 = \sqrt{2\nu/m}$ and minima at the well positions $\pm x_0 = \pm\sqrt{\nu/\beta}$. The two lowest energy eigenstates of the double-well potential are thus even and odd cat states, respectively. Preparing the system in either of them results in a quantum superposition of two macroscopically distinguishable states of a massive object, provided that x_0 exceeds the zero-point motion $x_{\rm zpm} = \sqrt{\hbar/2\omega_0 m}$ associated to the ground state of each well [27].

We now show how optomechanical sideband cooling can be used for ground state preparation in such a highly nonlinear potential. Since the coupling to a thermal environment ensures that the populations of the double-well eigenstates decay exponentially with the energy, it would in principle be sufficient to transfer all population of the first excited state to the ground state. In practice, however, it is challenging to generate a sufficient cooling rate for the lowest transition. The (linearized) coupling between the mechanical oscillator and a cavity electromagnetic mode with annihilation operator $\hat{a}$ and frequency ω_c takes the form $\hbar g \hat{x}(\hat{a} + \hat{a}^\dagger)$, where $g = g_0\sqrt{\bar{n}_c}$, with $g_0 = (\partial\omega_c/\partial x)_{x=0}$ the bare optomechanical coupling and $\bar{n}_c$ the photon number induced in the cavity by an external field driving it at a frequency $\omega_c|_{x=0} + \Delta$ that allows us to control g [28,29]. Efficient ground state cooling requires essentially three conditions: (i) the detuning Δ of the external driving field with respect to the cavity mode has to be chosen as $\Delta \approx -\delta_{10} \equiv (E_1 - E_0)/\hbar$, with (ii) a photon relaxation rate κ satisfying $\delta_{10} \gg \kappa \gg g_{10}$, while (iii) keeping the cooperativity $g_{10}^2/\kappa\gamma_{10}\bar{N}(\delta_{10})$ large enough (here $g_{10} = g\langle 1|\hat{x}|0\rangle$ is the optomechanical coupling rate for the lowest mechanical transition, γ_{10} is the relaxation

rate of the transition, and $\bar{N}(\Omega)$ are the thermal environmental excitations at the corresponding frequency, see below). Yet, as δ_{10} decreases exponentially with the separation between the wells, the cooperativities and cooling rates generated in this way would be rather limited.

To obtain more efficient cooling, the mechanical system can be coupled to a set of cavity modes with relaxation rates κ_j, each performing sideband cooling in one or more transitions as illustrated in Fig. 1. As we show numerically, this arrangement cools down the mechanical mode close to its ground state even for moderate relaxation rates $\kappa_j \lesssim \delta_{mn}$, where $\delta_{mn} = (E_m - E_n)/\hbar > 0$ refers to the transition we intend to cool with mode j. For realizations where all employed cavity modes have comparable linewidths κ_j, as is the case in most settings, the performance of this cooling concept improves with the number of modes. This may, however, face practical limitations (see below). We remark that our approach does not only apply to model (1) but to any nonlinear potential with a nondegenerate ground state.

In the following, we will describe the system via a master equation for its state $\hat{\rho}$. Whereas the dissipation of photons can be treated in the common way, the nonlinearity of the mechanical motion requires special attention. As a master equation is based on a perturbative expansion in system-environment couplings, it here leads to nonunitary terms of Lindblad form for each transition between eigenstates of the mechanical mode [30–34], since each transition couples with a different strength to the environment and experiences a different density of states. Using an adequate "microscopic" model for the system-environment interaction, we thus derive the master equation [34],

$$\partial_t\hat{\rho} = \frac{1}{i\hbar}[\hat{H},\hat{\rho}] + \frac{\kappa}{2}\sum_j \mathcal{D}_{\hat{a}_j}[\hat{\rho}] + \frac{1}{2}\mathcal{L}_m[\hat{\rho}], \qquad (2)$$

where $\hat{H} = \hat{H}_{\rm DW} + \sum_j[-\hbar\Delta_j\hat{a}_j^\dagger\hat{a}_j + \hbar g_j(\hat{a}_j + \hat{a}_j^\dagger)\hat{x}]$ is the full Hamiltonian and $\mathcal{D}_{\hat{O}}[\cdot] = 2\hat{O}(\cdot)\hat{O}^\dagger - \hat{O}^\dagger\hat{O}(\cdot) - (\cdot)\hat{O}^\dagger\hat{O}$ a standard Lindblad superoperator. $\mathcal{L}_m[\cdot] = [\hat{x},(\cdot)\hat{A}^\dagger - \hat{A}(\cdot)]$ is the mechanical dissipator [34] with

$$\hat{A} = \sum_{m>n}\gamma_{mn}k_{mn}[\bar{N}(\delta_{mn})|m\rangle\langle n| + [\bar{N}(\delta_{mn}) + 1]|n\rangle\langle m|],$$

where $\gamma_{mn} = \delta_{mn}/Q$ is the $|m\rangle \to |n\rangle$ decay rate and $\bar{N}(\Omega) = [\exp(\hbar\Omega/k_{\rm B}T) - 1]^{-1}$ the reservoir occupation at temperature T and frequency Ω. Q is the quality factor of harmonic mechanical oscillations and $k_{mn} = x_{mn}(2m\omega/\hbar)$ are the position matrix elements normalized to the zero-point position variance associated to the original harmonic oscillations, see below. We now turn to propose a specific implementation of these ideas, for which a realistic choice of parameters allows us to cool the mechanical mode to the ground state showing the desired superposition.
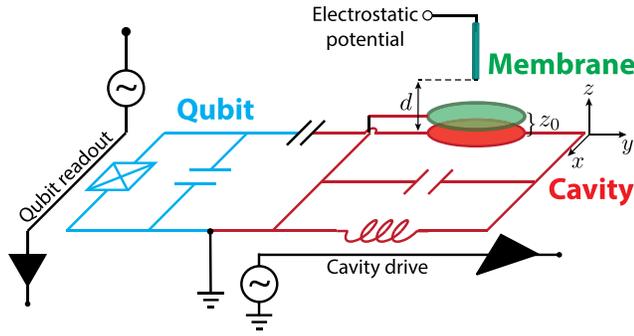
FIG. 2. Scheme for the circuit quantum electromechanical implementation of our proposal. The mechanical membrane (green) alongside a disk electrode of a microwave cavity (red) produces a position-dependent capacitance, and hence an optomechanical coupling to the cavity modes. A superconducting qubit (blue) is capacitively coupled to the cavity, and we employ it for reading out the mechanical state. The double-well potential is engineered on the membrane through an electrostatically fed electrode tip placed above its center, which produces a softening potential.

Implementation.—To implement our ideas, we here propose an architecture based on state-of-the-art superconducting circuits and electromechanical technology, see Fig. 2 and Ref. [42] for a similar device. In this proposal, the mechanical degree of freedom is realized by the drum mode of a thin circularly clamped mechanical layer (membrane) of radius a, which is confined in a double-well potential generated via the electrostatic field of a tip electrode located above its center. The cavity modes, in turn, are the resonance modes of a superconducting resonator with a disk-shaped end placed below the membrane such that plate and membrane form a capacitance. The dependence of its capacitance on the plate-to-membrane separation then provides the desired optomechanical interaction. An additional superconducting qubit coupled to the microwave resonator will allow us to read out the mechanical motion.

Let us now elaborate on the physics behind this scenario. In [34] we provide a detailed derivation of the Hamiltonian describing the membrane. The fundamental flexural mode with position $\hat{x}$ and momentum $\hat{p}$ is found to be well isolated from the rest of the mechanical modes and, besides a harmonic restoring potential with frequency ω, it is subject to a nonlinear potential of geometric origin that is, to leading order, well described by a Duffing nonlinearity of the form $\beta\hat{x}^4/4$. The total elastic potential $\hat{V}_m = m\omega^2\hat{x}^2/2 + \beta\hat{x}^4/4$ can be transformed into a double well of the form (1) by adding a "softening" force which generates an additional potential with the shape of an inverted parabola that exceeds the harmonic confinement in $\hat{V}_m$. A feasible way to controllably generate such a force on the membrane consists of applying an inhomogeneous electrostatic field generated via a tip electrode situated close to its center, see Fig. 2. The electrostatic energy

of the membrane's fundamental mode can be expanded in its deflection, $\hat{V}_{es} = \sum_{j=1}^{\infty} \alpha_j \hat{x}^j$, with coefficients $\alpha_j = \pi h \epsilon_0 \int_0^a r dr \partial_z^j E_z^2(r, z=z_0)\psi_0^j(r)$ [34]. Here, ψ_0 is the profile of the fundamental mode, E_z is the static electric-field component perpendicular to the mechanical layer, and h is the membrane's thickness at rest in the $z = z_0$ plane ($z = 0$ is taken at the superconducting disk below the membrane). α_1 shifts the equilibrium position of the mechanical mode and can be used as an additional control knob for the coupling to the electromagnetic modes [43]. α_2 can be made negative, therefore generating the softening force that leads to the double-well potential. Higher orders are shown to be negligible [34]. Hence, we see that the combination of the geometrical and electrostatic potentials, $\hat{V}_m + \hat{V}_{es}$, gives rise to the desired double-well potential for the membrane's motion, with a parameter $\nu = 2|\alpha_2| - m\omega^2$ that can be tuned via the applied electrostatic fields.

As ideally suited candidates for the mechanical elements we here consider monolayer graphene sheets, since they have mechanical properties adapted to our needs. In particular, their ultralow mass provides them with large zero-point motion x_{zpm}, while their large Young modulus confers them large Duffing nonlinearity β. Such sheets have already been studied as mechanical resonators [43–45]. Importantly, we note that the low conductivity of graphene that has limited optomechanical cooling in these experiments can be overcome by doping the membrane surface with alkaline-metal atoms, as has been recently shown with lithium-decorated graphene sheets [46], which possess almost the same mechanical properties as standard monolayer graphene [47] but are superconducting [48].

We now turn to discuss the achievable fidelity for preparing stationary spatial-superposition states with our approach for parameters corresponding to this specific implementation. The superconducting gap imposes a limit to the number of high quality resonance modes in the cavity. We thus consider three cavity modes coupled to three proper mechanical transitions. Assuming the same decay rate $\kappa = \kappa_j$ ($j = 1, 2, 3$) for all these modes, we tune the optomechanical couplings g_j such that the probability of being in the ground state of the double well is maximized.

Results.—We consider a monolayer lithium-decorated graphene sheet with radius $a = 1 \mu$m, and thus $m \approx 5.7 \times 10^{-16}$ g, $\omega/2\pi \approx 26$ MHz, and $\beta \approx 5.7 \times 10^{15}$ J/m^4 [34,44]. The distance between the membrane and the disk-shaped end of the cavity is taken to be $z_0 = 100$ nm. For a cavity with fundamental resonance at 5 GHz we get the "bare" optomechanical coupling rate $G_0 = g_0\sqrt{\hbar/2m\omega} \approx 2\pi \times 10$ Hz. As G_0 scales linearly with the diameter of the membrane [43], its small radius should be compensated by an increased intracavity photon number $\bar{n}_c$. The electrostatic field is adjusted such that $\alpha_2 = -1.000\,134(m\omega^2/2)$,

which requires the application of a few hundred volts to an antenna of a few hundred nanometers in size (similar to the tip of a scanning tunneling microscope) located about 1 μm above the center of the membrane, and creates a shallow double well with only two levels below the barrier, cf. Fig. 1(a). This situation assures a reasonably large value of δ_{10} ($\sim 2\pi \times 50$ kHz) that allows us to access the required resolved sideband regime.

We numerically [49] obtain the steady-state solution $\bar{\rho}$ of the master equation (2), and analyze the ground state population $P_{00} = \langle 0|\bar{\rho}_m|0\rangle$ present in the reduced mechanical state $\bar{\rho}_m = \text{Tr}_{\text{cavity}}\{\bar{\rho}\}$. We consider three cavity modes with decay rates $\kappa = 0.3\delta_{10}$, detunings matching the mechanical transitions $|1\rangle \leftrightarrow |0\rangle$, $|3\rangle \leftrightarrow |0\rangle$, and $|2\rangle \leftrightarrow |1\rangle$ (i.e., $\Delta_1 = -\delta_{10}$, $\Delta_2 = -\delta_{30}$, and $\Delta_3 = -\delta_{21}$), and optimized intracavity photon numbers $\bar{n}_{c1} = 1200$, $\bar{n}_{c2} = 1100$, and $\bar{n}_{c3} = 4000$ [34]. Note that only transitions with $x_{mn} \neq 0$ can be cooled, which requires m and n to have different parity [34]. Assuming an environment temperature of $T = 15$ mK and a quality factor $Q = 10^6$ of the membrane in the original approximately harmonic potential $\hat{V}_m$, we obtain $P_{00} \approx 0.79$, meaning that the mechanical resonator can be found in the desired spatial-superposition state with $\sim 79\%$ probability [Fig. 3(a)]. This nonequilibrium steady state of the mechanical mode has a spatial extent equal to the separation of the wells, whose ratio to the zero-point motion amplitude in each well is $2x_0/x_{\text{zpm}} \approx 6$. It is reached in about 30 μs, which is orders of magnitude shorter than the time scales of fluctuations in the electrostatic control fields or microwave tones, see Ref. [50]. Larger probabilities can be obtained by working deeper in the resolved sideband regime and/or by employing more cavity modes.

To show how our proposal could be exploited for the examination of unconventional sources of decoherence, let us consider the bounds it imposes on the continuous
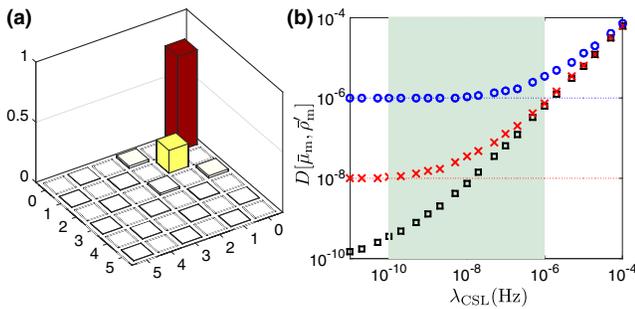

FIG. 3. (a) Absolute value of the lowest elements of the mechanical steady-state density matrix when cooled by three electromagnetic modes with optimal detunings and optomechanical couplings as explained in the text. (b) Distance between the population distributions of steady states $\bar{\rho}'_m$ and $\bar{\mu}_m$ in the absence or presence of CSL versus localization rate λ_{CSL} for measurement precision $\sigma = 10^{-6}$ (circles), 10^{-8} (crosses), and 10^{-10} (squares). The shaded area is the predicted range for λ_{CSL} [2,51,52].

spontaneous localization (CSL) model [2,51,52] as the most prominent collapse model. The CSL model is characterized by a localization length usually taken to be $r_{\text{CSL}} = 100$ nm, and a localization rate which is predicted to be in the $\lambda_{\text{CSL}} = 10^{-8 \pm 2}$ Hz range [2]. In the limit where the delocalization amplitude x_0 is much smaller than r_{CSL}, the effect of the CSL model can be approximated by a momentum diffusion term (CSL diffusion) of the form $-(\lambda_{\text{CSL}}\eta/r_{\text{CSL}}^2)[\hat{x},[\hat{x},\hat{\rho}]]$ ($\eta \approx 1.2 \times 10^{15}$ is a mass and geometry dependent factor [53]) to be added to Eq. (2).

Our setup can be used to distinguish CSL diffusion from conventional sources of noise by revealing the differences between the steady states in the presence and absence of CSL. To this end, one would proceed as follows. After a sufficient experimental characterization of the setup, i.e., its mechanical spectrum, optomechanical couplings, etc., one can infer the mechanical damping in a sideband cooling experiment, see, e.g., [54,55]. Whether only the assumed mechanical damping or possibly also CSL is present in the experiment can then be determined by measuring several matrix elements of the mechanical steady state, see below for a measurement method. To quantitatively analyze this procedure we calculated the steady state $\bar{\mu}_m$ for a mechanical quality factor Q in the presence of CSL and the steady state $\bar{\rho}'_m$ in the absence of CSL but with a mechanical quality factor $Q' < Q$, chosen such that the ground state occupations are equal $\langle 0|\bar{\rho}'_m|0\rangle = \langle 0|\bar{\mu}_m|0\rangle$. To mimic a finite measurement precision σ, we only require that $|\langle 0|\bar{\rho}'_m|0\rangle - \langle 0|\bar{\mu}_m|0\rangle| \lesssim \sigma$. Crucially, the CSL diffusion rate $\lambda_{\text{CSL}}\eta/r_{\text{CSL}}^2$ is independent of the mechanical spectrum, whereas the thermal damping rates γ_{mn} strongly depend on the anharmonicity of the potential [34]. As a consequence, the occupation probabilities of excited mechanical states differ, i.e., $|\langle j|\bar{\rho}'_m|j\rangle - \langle j|\bar{\mu}_m|j\rangle| \gg \sigma$ for $j \geq 1$ and sufficiently large λ_{CSL}, indicating that the modified steady state cannot be accounted for by a reduced quality and other sources of decoherence need to be invoked. To quantify these differences we use the distance between the distributions of the mechanical occupations, $D[\bar{\mu}_m, \bar{\rho}'_m] = \sqrt{\sum_{n=0}^{\infty} \langle n|(\bar{\mu}_m - \bar{\rho}'_m)|n\rangle^2}$, which is plotted as a function of λ_{CSL} for three different measurement precisions $\sigma = 10^{-6}$, 10^{-8}, and 10^{-10} in Fig. 3(b).

Of course, the above discussion assumes that the mechanical damping is of a specific form. Yet due to the ample tunability of our setup, other forms of mechanical damping may also be identified and distinguished from CSL as long as they are not exactly in the form of a momentum diffusion with a rate that is independent of the potential.

State verification.—As the verification of the prepared states will be of crucial importance in experiments, we now introduce a strategy that allows us to determine all elements P_{mn} of steady-state mechanical density matrix $\bar{\rho}_m = \sum_{mn} P_{mn}|m\rangle\langle n|$, for which $x_{mn} \neq 0$, and the diagonal elements P_{nn}, see [34] for the details. We exploit the fact

that our proposed architecture is naturally suited to strongly couple the electromagnetic cavity to a superconducting qubit with ground and excited states $|g\rangle$ and $|e\rangle$, and a transition frequency that can be tuned *in situ* and in real time (e.g., via a time dependent external magnetic flux for transmon and phase qubits [56,57]). Measurements of the qubit's population will allow us to read out the mechanical density matrix as follows.

Using an electromagnetic mode that is far detuned from the qubit and mechanical transitions (dispersive regime), one obtains an effective qubit-mechanical interaction of the form $\hat{x}\hat{\sigma}_x$, where $\hat{\sigma}_x = |g\rangle\langle e| + |e\rangle\langle g|$. We show in [34] that by initializing the qubit in the ground state, and tuning its frequency to the $|m\rangle \leftrightarrow |n\rangle$ transition ($m > n$), the probability of finding it in the excited state oscillates in time with an amplitude proportional to the diagonal element P_{mm} of the mechanical density matrix. On the other hand, by initializing the qubit in the superposition $|g\rangle + e^{i\varphi}|e\rangle$, the excitation probability becomes sensitive to $i(P_{mn}e^{i(\phi_{mn}-\varphi)} - \text{c.c.})$, where ϕ_{mn} is the phase of x_{mn}, hence allowing for the determination of the real and imaginary parts of the off-diagonal elements P_{mn} via a proper choice of φ.

Conclusion.—We have introduced a method for the steady-state preparation of spatial quantum superposition of a macroscopic object. Our proposal is based on cooling a mechanical mode to the ground state of an engineered double-well potential. We have put forward a specific implementation based on current superconducting circuits and electromechanical technology together with a method for verifying the prepared mechanical state and discussed a strategy for testing the validity of the CSL model. The methods and specific proposal introduced in this Letter pave the way towards the generation of macroscopic spatial superpositions with available modern technologies, that allow us to put bounds on collapse models and shed light on the quantum-to-classical transition.

[1] W. H. Zurek, Phys. Today **44**, 36 (1991).

[2] A. Bassi and G. Ghirardi, Phys. Rep. **379**, 257 (2003).

[3] J. Ellis, S. Mohanty, and D. V. Nanopoulos, Phys. Lett. B **221**, 113 (1989).

[4] R. Penrose, Gen. Relativ. Gravit. **28**, 581 (1996).

[5] A. Frenkel, Found. Phys. **20**, 159 (1990).

[6] M. Arndt and K. Hornberger, Nat. Phys. **10**, 271 (2014).

[7] S. Bose, K. Jacobs, and P. L. Knight, Phys. Rev. A **59**, 3204 (1999).

[8] W. Marshall, C. Simon, R. Penrose, and D. Bouwmeester, Phys. Rev. Lett. **91**, 130401 (2003).

[9] K. C. Schwab and M. L. Roukes, Phys. Today **58**, 36 (2005).

[10] M. J. Hartmann and M. B. Plenio, Phys. Rev. Lett. **101**, 200503 (2008).

[11] A. Asadian and M. Abdi, Phys. Rev. A **93**, 052315 (2016).

[12] S. Savel'ev, X. Hu, and F. Nori, New J. Phys. **8**, 105 (2006).

[13] S. Rips, M. Kiffner, I. Wilson-Rae, and M. J. Hartmann, New J. Phys. **14**, 023042 (2012).

[14] S. Rips and M. J. Hartmann, Phys. Rev. Lett. **110**, 120503 (2013).

[15] O. Romero-Isart, A. C. Pflanzer, F. Blaser, R. Kaltenbaek, N. Kiesel, M. Aspelmeyer, and J. I. Cirac, Phys. Rev. Lett. **107**, 020405 (2011).

[16] O. Romero-Isart, L. Clemente, C. Navau, A. Sanchez, and J. I. Cirac, Phys. Rev. Lett. **109**, 147205 (2012).

[17] P. Werner and W. Zwerger, Europhys. Lett. **65**, 158 (2004).

[18] A. Voje, J. M. Kinaret, and A. Isacsson, Phys. Rev. B **85**, 205415 (2012).

[19] L. F. Buchmann, L. Zhang, A. Chiruvelli, and P. Meystre, Phys. Rev. Lett. **108**, 210403 (2012).

[20] R. Ghobadi, S. Kumar, B. Pepper, D. Bouwmeester, A. I. Lvovsky, and C. Simon, Phys. Rev. Lett. **112**, 080503 (2014).

[21] M. Abdi, M. Pernpeintner, R. Gross, H. Huebl, and M. J. Hartmann, Phys. Rev. Lett. **114**, 173602 (2015).

[22] J.-Q. Liao and L. Tian, Phys. Rev. Lett. **116**, 163602 (2016).

[23] M. Abdi, S. Pirandola, P. Tombesi, and D. Vitali, Phys. Rev. Lett. **109**, 143601 (2012).

[24] A. A. Clerk, F. Marquardt, and K. Jacobs, New J. Phys. **10**, 095010 (2008).

[25] S. Singh and P. Meystre, Phys. Rev. A **81**, 041804 (2010).

[26] M. R. Vanner, I. Pikovski, G. D. Cole, M. S. Kim, Č. Brukner, K. Hammerer, G. J. Milburn, and M. Aspelmeyer, Proc. Natl. Acad. Sci. U.S.A. **108**, 16182 (2011).

[27] C. Monroe, D. M. Meekhof, B. E. King, and D. J. Wineland, Science **272**, 1131 (1996).

[28] I. Wilson-Rae, N. Nooshi, W. Zwerger, and T. J. Kippenberg, Phys. Rev. Lett. **99**, 093901 (2007).

[29] F. Marquardt, J. P. Chen, A. A. Clerk, and S. M. Girvin, Phys. Rev. Lett. **99**, 093902 (2007).

[30] H.-P. Breuer and F. Petruccione, *The Theory of Open Quantum Systems* (Oxford University Press, Oxford, 2007).

[31] F. Beaudoin, J. M. Gambetta, and A. Blais, Phys. Rev. A **84**, 043832 (2011).

[32] A. Ridolfo, M. Leib, S. Savasta, and M. J. Hartmann, Phys. Rev. Lett. **109**, 193602 (2012).

[33] A. Ridolfo, S. Savasta, and M. J. Hartmann, Phys. Rev. Lett. **110**, 163601 (2013).

[34] See the Supplemental Material at http://link.aps.org/supplemental/10.1103/PhysRevLett.116.233604, which includes Refs. [35–41], for more details on the dynamics of the system under decoherence, the flexural modes of the membrane, the electrostatic softening, and the state verification of the membrane.

[35] L. D. Landau and E. M. Lifshitz, *Theory of Elasticity* (Pergamon Press, Bristol, 1975).

[36] A. M. Eriksson, D. Midtvedt, A. Croy, and A. Isacsson, Nanotechnology **24**, 395702 (2013).

[37] G. A. Steele, A. K. Hüttel, B. Witkamp, M. Poot, H. B. Meerwaldt, L. P. Kouwenhoven, and H. S. J. van der Zant, Science **325**, 1103 (2009).

[38] J. D. Jackson, *Classical Electrodynamics*, 3rd ed. (Wiley, Hoboken, 1998).

[39] K. R. Kganyago and P. E. Ngoepe, Phys. Rev. B **68**, 205111 (2003).

[40] R. A. Barton, B. Ilic, A. M. van der Zande, W. S. Whitney, P. L. McEuen, J. M. Parpia, and H. G. Craighead, Nano Lett. **11**, 1232 (2011).

[41] R. Barends, J. Kelly, A. Megrant, D. Sank, E. Jeffrey, Y. Chen, Y. Yin, B. Chiaro, J. Mutus, C. Neill, P. O'Malley, P. Roushan, J. Wenner, T. C. White, A. N. Cleland, and J. M. Martinis, Phys. Rev. Lett. **111**, 080502 (2013).

[42] F. Lecocq, J. D. Teufel, J. Aumentado, and R. W. Simmonds, Nat. Phys. **11**, 635 (2015).

[43] P. Weber, J. Güttinger, I. Tsioutsios, D. E. Chang, and A. Bachtold, Nano Lett. **14**, 2854 (2014).

[44] V. Singh, S. J. Bosman, B. H. Schneider, Y. M. Blanter, A. Castellanos-Gomez, and G. A. Steele, Nat. Nanotechnol. **9**, 820 (2014).

[45] X. Song, M. Oksanen, J. Li, P. J. Hakonen, and M. A. Sillanpää, Phys. Rev. Lett. **113**, 027404 (2014).

[46] B. M. Ludbrook, G. Levy, P. Nigge, M. Zonno, M. Schneider, D. J. Dvorak, C. N. Veenstra, S. Zhdanovichb, D. Wong, P. Dosanjh, C. Straßer, A. Stöhr, S. Forti, C. R. Ast, U. Starke, and A. Damascelli, Proc. Natl. Acad. Sci. U.S.A. **112**, 11795 (2015).

[47] Y. Qi, H. Guo, L. G. Hector, Jr., and A. Timmons, J. Electrochem. Soc. **157**, A558 (2010).

[48] G. Profeta, M. Calandra, and F. Mauri, Nat. Phys. **8**, 131 (2012).

[49] C. Navarrete-Benlloch, arXiv:1504.05266.

[50] S. Rips, I. Wilson-Rae, and M. J. Hartmann, Phys. Rev. A **89**, 013854 (2014).

[51] M. Bahrami, M. Paternostro, A. Bassi, and H. Ulbricht, Phys. Rev. Lett. **112**, 210404 (2014).

[52] A. Vinante, M. Bahrami, A. Bassi, O. Usenko, G. Wijts, and T. Oosterkamp, Phys. Rev. Lett. **116**, 090402 (2016).

[53] S. Nimmrichter, K. Hornberger, and K. Hammerer, Phys. Rev. Lett. **113**, 020405 (2014).

[54] A. Jöckel, M. T. Rakher, M. Korppi, S. Camerer, D. Hunger, M. Mader, and P. Treutlein, Appl. Phys. Lett. **99**, 143109 (2011).

[55] S. Groblacher, A. Trubarov, N. Prigge, G. D. Cole, M. Aspelmeyer, and J. Eisert, Nat. Commun. **6**, 7606 (2015).

[56] J. Majer, J. M. Chow, J. M. Gambetta, J. Koch, B. R. Johnson, J. A. Schreier, L. Frunzio, D. I. Schuster, A. A. Houck, A. Wallraff, A. Blais, M. H. Devoret, S. M. Girvin, and R. J. Schoelkopf, Nature (London) **449**, 443 (2007).

[57] M. Hofheinz, E. M. Weig, M. Ansmann, R. C. Bialczak, E. Lucero, M. Neeley, A. D. O'Connell, H. Wang, J. M. Martinis, and A. N. Cleland, Nature (London) **454**, 310 (2008).